ORIGINAL RESEARCH

Novel Tissue-Specific Multifunctionalized Nanotechnological Platform Encapsulating Riluzole Against Motor Neuron Diseases

Gerard Esteruelas [1–3], Miren Ettcheto [4–7], Isabel Haro [3], Mireia Herrando-Grabulosa [8,9], Núria Gaja-Capdevila [8,9], Maria Jose Gomara [3], Xavier Navarro [8,9], Marta Espina [1,2], Eliana B Souto [10], Antoni Camins [4–6], Maria Luisa García [1,2,5], Elena Sánchez-López [1–3,5]

[1]Department of Pharmacy, Pharmaceutical Technology and Physical Chemistry, Faculty of Pharmacy and Food Sciences, University of Barcelona, Barcelona, 08028, Spain; [2]Institute of Nanoscience and Nanotechnology (IN2UB), University of Barcelona, Barcelona, 08028, Spain; [3]Unit of Synthesis and Biomedical Applications of Peptides, IQAC-CSIC, Barcelona, 08034, Spain; [4]Department of Pharmacology and Therapeutic Chemistry, Faculty of Pharmacy and Food Sciences, University of Barcelona, Barcelona, Spain; [5]Biomedical Research Network Center in Neurodegenerative Diseases (CIBERNED), Madrid, Spain; [6]Institute of Neuroscience, Universitat de Barcelona, Barcelona, Spain; [7]Institute of Pere Virgili Health Research (IISPV), Reus, Spain; [8]Group of Neuroplasticity and Regeneration, Department of Cell Biology, Universitat Autonoma de Barcelona, Barcelona, Spain; [9]Physiology and Immunology, Institute of Neurosciences, Universitat Autonoma de Barcelona, Barcelona, Spain; [10]UCD School of Chemical and Bioprocess Engineering, University College Dublin, Belfield, Dublin, D04 V1W8, Ireland

Correspondence: Maria Luisa García; Elena Sánchez-López, Email marisagarcia@ub.edu; esanchezlopez@ub.edu

Background: Motor neuron diseases are neurological disorders characterized by progressive degeneration of upper and/or lower motor neurons. Amyotrophic Lateral Sclerosis (ALS) is the most common form of motor neuron diseases, where patients suffer progressive paralysis, muscle atrophy and finally death. Despite ALS severity, no treatment is safe and fully effective. In this area, Riluzole was the first drug approved and it constitutes the gold-standard for this pathology. However, to obtain suitable therapeutic efficacy, Riluzole requires high doses that are associated with severe adverse effects in other tissues. To attain Riluzole therapeutic efficacy avoiding other organs side-effects, new therapeutic strategies to enhance the delivery of Riluzole specifically to motor neurons constitute an unmet medical need. In this area, we have developed a novel multifunctional nanostructurated carrier to selectively deliver Riluzole to motor neurons.

Results: This work develops and characterizes at in vitro and in vivo levels a tissue-targeted formulation of peptide and PEG-labelled PLGA nanoparticles encapsulating Riluzole. For this purpose, pVEC, a cell penetrating peptide able to increase transport through the blood–brain barrier, was attached to the nanoparticles surface. The multifunctionalized nanoparticles show suitable characteristics for the release of Riluzole in the central nervous system and were detected in motor neurons within 1 h after administration while significantly reducing the concentration of Riluzole in non-therapeutic organs responsible of side effects.

Conclusion: A novel drug delivery system has been developed and characterized, demonstrating enhanced CNS biodistribution of riluzole, which shows promise as efficient therapeutic tool for motor neuron diseases, including amyotrophic lateral sclerosis.

Keywords: motor neuron disease, nanomedicine, PLGA-PEG, pVEC, riluzole, drug delivery system

Introduction

Motor neuron diseases (MNDs) encompass a collection of neurodegenerative disorders characterized by the progressive deterioration of motor neurons (MNs). This degeneration leads to the gradual loss of neuromuscular junctions, resulting in muscle denervation and atrophy.[1] Most MNDs are classified as rare pathologies, impacting fewer than 5 individuals per 10,000. Despite their rarity, this group of diseases affects between 6% and 10% of the European population, presenting a significant global health concern.[2,3] MNDs inflict severe disability and carry a high mortality rate, affecting both children and adults. They typically manifest as progressive muscle atrophy, beginning in the limbs and eventually extending to impair functions such as swallowing and respiration, ultimately culminating in death.[1,4] MNDs include

Graphical Abstract
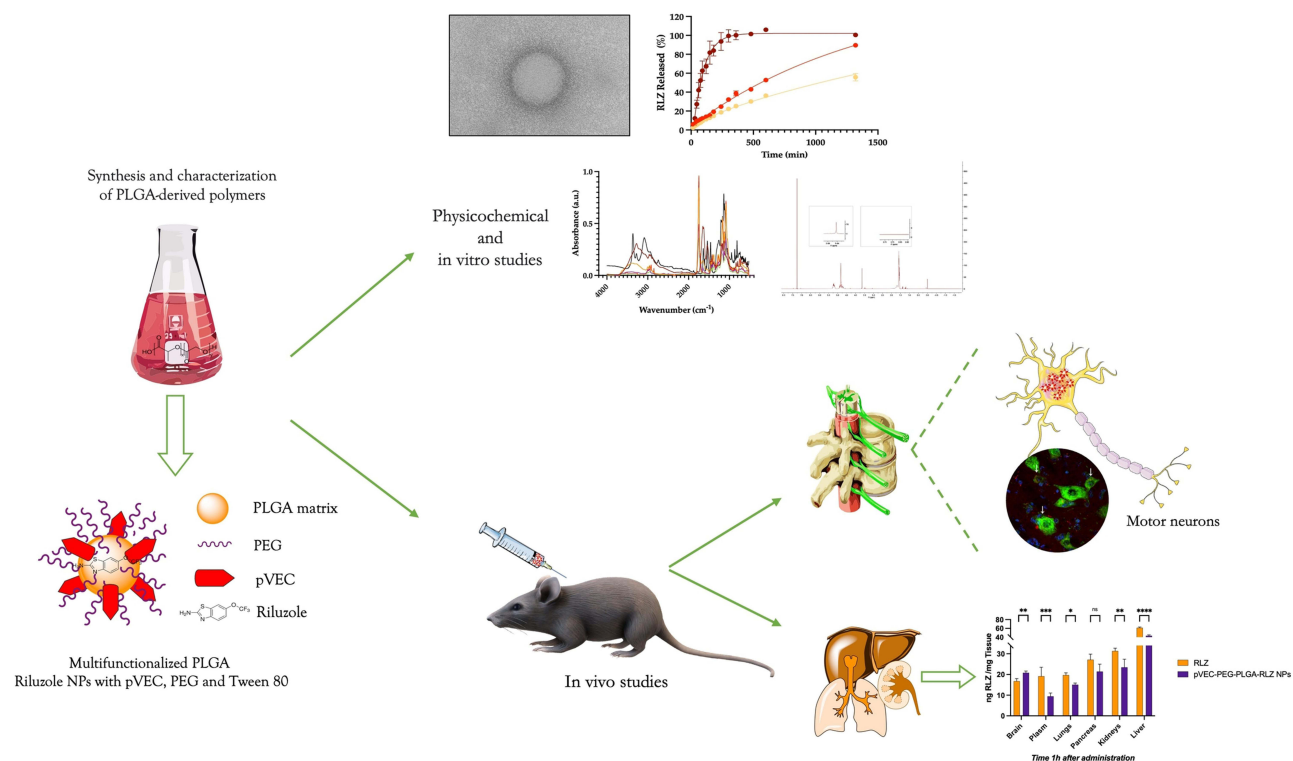
numerous conditions, but Amyotrophic Lateral Sclerosis (ALS) stands out as the most common in adult population.[5,6] Presently, ALS carries a devastating prognosis, typically leading to death within 2 to 4 years after diagnosis.[7]

Riluzole (RLZ) is a drug classified within the benzothiazole group, functioning as a neuroprotective agent. Its mechanism of action involves mitigating excitotoxicity by inhibiting glutamate transmission at the postsynaptic level.[8,9] Currently, RLZ is commercially marketed for the treatment of ALS. Although it cannot reverse or cure the disease, recent research has suggested that RLZ may be more effective than initial studies indicated, mildly prolonging the life of the patients and improving neuromuscular function.[10–12] Moreover, RLZ possesses a positive effect on the psychological well-being of patients, reducing anxiety, depression and compulsive disorders.[11–13] However, in clinical practice, the therapeutic effectiveness of RLZ may be limited because high doses are required to maintain a therapeutic concentration in the central nervous system (CNS), which may result in adverse effects such as hepatotoxicity, respiratory or cardiac problems, among others.[14,15]

In order to overcome these drawbacks, the encapsulation of RLZ in a platform able to transport it to the CNS targeting MNs, avoiding other organs side effects and providing a prolonged release, may constitute a suitable therapeutic strategy. In this area, polymeric nanoparticles (NPs) composed of a central Poly-L-lactic-co-glycolic acid (PLGA) core had previously demonstrated their capacity to encapsulate RLZ.[16] However, in order to achieve an effective functionalization, combination of both passive and active targeting constitute key strategies. Therefore, a dual passive targeting aimed firstly to facilitate NPs blood–brain barrier (BBB) penetration, and secondly to reduce NPs interaction with the reticuloendothelial system decreasing their clearance has been attempted using Tween 80® and PEG, respectively.[16–21] Direct active targeting may be achieved using several molecules, being cell penetrating peptides (CPPs) one of the most suitable approaches.[22,23] CPPs can be custom-synthesised to be attached to PLGA chains and target MNs. Among several peptides, pVEC is a 18-amino acid amphipathic-cationic CPP derived from vascular endothelial cadherin,[24,25] which exhibits a penetration mechanism based on direct translocation. Moreover, pVEC has excellent properties for the

treatment of MNDs. Unlike other CPPs commonly used for the functionalization of polymeric NPs, such as SynB3, Tat 47–57, TET or polyarginine, pVEC shows higher penetration rate into the CNS and it is not significantly affected by CNS efflux mechanisms.[26] pVEC has demonstrated efficient cellular internalization, enabling the transport of large molecular cargoes, and further studies have shown that pVEC tends to accumulate in neurons, confirming target specificity for MNDs.[27]

In this work, two different co-polymers based on PLGA have been prepared. First, novel covalent binding between the custom-synthesised CPP pVEC and PLGA was achieved developing pVEC-PLGA. Furthermore, PEG was covalently linked to PLGA polymer (PEG-PLGA). Nanoparticles encapsulating RLZ were prepared using this two co-polymers being able to employ both active and passive strategies (pVEC-PEG-PLGA-RLZ NPs). Therefore, specific pVEC-PEG-PLGA-RLZ NPs were developed and physicochemically and morphologically characterized. Drug-interaction studies as well as RLZ in vitro release were also analyzed. Moreover, biodistribution and pharmacokinetics of pVEC-PEG-PLGA-RLZ NPs had also been assessed in rodent models, confirming that fluorescently labeled pVEC-PEG-PLGA-RLZ NPs arrive to spinal cord MNs.

Materials and Methods

Materials

PLGA 503H was obtained from Evonik Industries (Essen, Germany), PLGA-MAL and CH$_3$-PEG were purchased from Nanosoft Polymers (Winston-Salem, USA), RLZ by Thermo Fisher Scientific, (Pittsburgh, USA) 1-ethyl-3-(3-dimethyl-laminopropyl) carbodiimide hydrochloride (EDC), N-hydroxysuccinamida (NHS), Peptide-synthesis-grade trifluroacetic acid (TFA) and dimethylformamide (DMF) were obtained from Scharlau (Barcelona, Spain). HPLC-grade acetonitrile (CH$_3$CN) were from Fisher Scientific (Loughborough, UK). Acetic acid and hydrochloric acid were purchased from Panreac (AppliChem GmbH, Darmstadt, Germany). 2-(1H-7-azabenzotriazole-1-yl)-1,1,3,3-tetramethyluronium hexa-fluorophosphate methanaminium (HATU), was acquired from GenScript (Piscataway, USA). N,N-Diiso-propylethylamine (DIPEA), piperidine, triisopropylsilane (TIS), were from Sigma-Aldrich (Merck KGaA, Darmstadt, Germany), NovaSyn TGR resin and 9-fluorenyl-methoxycarbonyl (Fmoc) protected amino acids were purchased from Novabiochem (Merck Millipore, Merck KGaA, Darmstadt, Germany). All other reagents used were of analytical grade.

PLGA-PEG Synthesis

To obtain PLGA-PEG, PLGA activation was performed by mixing 50 µM PLGA 503H, 352 µM NHS and 352 µM EDC dissolved in chloroform, leaving it to react overnight. The polymer was then precipitated by adding 25 mL of diethyl ether and centrifuged at 4000 rpm for 8 minutes at 4°C. After removal of the supernatant, the pellet was dried with N$_2$ gas and dissolved in 4 mL of chloroform. This washing cycle was repeated three times. Finally, the activated PLGA (PLGA-NHS) was lyophilized and stored. Briefly. PLGA-NHS reacted with a molar equivalent of m-PEG-NH$_2$ and 352 µM N, N-diisopropylethylamine (DIEA) under stirring overnight. For the washing/precipitation cycles, a cold mixture of methanol : ethyl ether in a 20:80 ratio was used, centrifuging at 8000 rpm for 10 min at 4°C. Subsequently, the polymer obtained was dried with nitrogen gas, lyophilized and stored at −20°C.[20,28–30]

The binding of m-PEG to PLGA was confirmed by hydrogen nuclear magnetic resonance (^{1}H-NMR) spectroscopy. The polymer was dissolved in deuterated chloroform and the spectrum was obtained at 298 K on a Varian Inova 500 MHz spectrometer (Agilent Technologies, Santa Clara, CA, USA).

pVEC Synthesis

pVEC CPP was custom-synthesized by adding an extra C-terminal cysteine. As previously described by Vasconcelos et al,[31] this additional amino acid allowed subsequent binding of pVEC to the polymer. The peptide was synthesized by a 9-fluorenylmethoxycarbonyl/t-butyl (Fmoc/tBut) orthogonal protection strategy using manual solid-phase synthesis on a NovaSyn® TGR resin (0.23 mmol·g^{-1}).[32]

The coupling reactions were carried out by allowing a solution with a three-fold molar excess of the Fmoc-L-amino acids previously activated with HATU and DIEA,[33] dissolved in dimethylformamide, to react for

1 h. Subsequently, deprotection of the Fmoc group of the coupled amino acid was performed by adding DMF with 20% (v/v) piperidine twice for 10 min. The whole coupling/deprotection process was controlled for the primary amines using the Kaiser test, while for the secondary amine the Chloranyl test was used, which allow reliable detection of these groups.[33]

For the cleavage of the peptide side chain and release of the resin, a cleavage solution composed of 94.0% (v/v) TFA, 2.5% (v/v) H_2O MilliQ, 2.5% (v/v) 2-mercaptoethanol and 1% (v/v) triisopropylsilane was added to the peptidyl-resin and allowed to react for 4 h. Subsequently, TFA was removed by evaporation with N_2, the peptide was precipitated with cold ethyl ether and centrifuged for 10 min at 4000 rpm at 4°C. After 3 cycles of precipitation and centrifugation, the pellet was frozen in 10% acetic acid solution and lyophilized. The peptide obtained was stored at −20°C in a reducing argon atmosphere.[33]

The synthesized pVEC was analyzed by high-performance liquid chromatography (HPLC), using a Kromasil® C18 column (5 μm, 150 × 4.6 mm), with a 20 min gradient starting with 95% water (0.1% TFA) and ending with 95% acetonitrile (0.1% TFA). The peptide was also analyzed by Waters ACQUITY UPLC (Waters Corporation, Milford, MA, USA) with a UV-Vis and an electrospray ionization mass spectrometry (ESI-MS), Waters LCT Premier XE (Micromass Waters, Milford, MA, USA).

Conjugation and Characterization of PLGA-pVEC

Conjugation of pVEC with PLGA was also carried out. For this purpose, the N-terminal cysteine that has been incorporated into pVEC was left to react together with the maleimide group of PLGA-MAL.[31] A previously optimized concentration of 1.9 mg/mL PLGA-MAL and 0.89 mg/mL pVEC were completely dissolved in a solution of 1,1,1,3,3,3-Hexafluoro-2-propane/chloroform 80:20 and left under magnetic stirring for 18–24 h. Subsequently, the solvent was removed by evaporation under N_2 atmosphere and the peptide functionalized polymer was precipitated with cold diethyl ether. It was then centrifuged at 4000 rpm for 10 min at 4°C, lyophilized and stored at −20°C. It was then ultracentrifuged with a 3 kDa Amicon® filter in order to separate both PLGA-MAL and unbound pVEC, which was quantified using the HPLC methodology described in the previous section. Following this methodology, the amount of each component to be used for the PLGA-pVEC conjugation was optimized. Prior to ^{1}H-NMR characterization using Bruker AV-III-500-HD 500 MHz equipment, PLGA-pVEC was dissolved in DMSO-d6.

Obtention and Characterization of pVEC-PEG-PLGA-RLZ NPs

Preparation of pVEC-PEG-PLGA-RLZ NPs was carried out using the solvent displacement method.[16,34] Composition of the formulation was based on a previous work.[16] However, in the present work, from the 8 mg/mL of PLGA, 45% corresponded to non-functionalized PLGA, 45% to PLGA-PEG and 10% to PLGA-PVEC. These amounts were dissolved along with 1.5 mg/mL RLZ in acetone to form the organic phase. This organic phase was added dropwise to the aqueous phase composed of 3.5% Tween at pH 5. Subsequently, acetone was removed from the pVEC-PEG-PLGA -RLZ NPs by evaporation under reduced pressure.

Average size (Z_{av}) and polydispersity index (PI) were determined by 1:10 dilution in H_2O MilliQ using photon correlation spectroscopy with a Zetasizer Nano ZS (Malvern Instruments, Malvern, UK) at 25°C.[35] For zeta potential (ZP) measurements, the sample was diluted 1:20 and determined by electrophoretic mobility using a Zetasizer Nano ZS. All measurements were carried out in triplicate.

Entrapment efficiency (EE) was analyzed indirectly by determining the amount of free RLZ by reverse-phase HPLC under isocratic conditions using a Kromasil® C18 column (5 μm, 150 × 4.6 mm) with a flow rate of 1 mL/min and a ratio of 70:30 methanol:H_2O MilliQ at 264 nm. Prior to chromatographic analysis, NPs were diluted 1:5 in MilliQ H_2O and filtered using Ultra 0.5 centrifugal filtration devices (Amicon® Millipore Corporation, Ireland) at 14000 rpm for 15 min.

For morphological analysis, transmission electron microscopy (TEM, Jeol 1010) was used to reveal the presence and morphology of the nanoparticles. Copper grids activated with UV light were used and samples were applied on the grid surface. 2% (w/v) uranyl acetate was used for negative staining as described in previous studies.[36,37]

Interaction Studies

The crystalline or amorphous state, as well as the interactions and molecular changes of the pVEC-PEG-PLGA-RLZ NPs and the different synthesized polymers, were studied by X-Ray diffraction (XRD) and Fourier-transformed infrared (FTIR) techniques. XRD spectra were obtained by exposing the samples to CuK radiation (45 kV, 40 mA, λ = 1.5418 Å) over a range of angles (2θ) from 2° to 60°, with a step of 0.026 and a time measurement of 200 s per step.[38] For FTIR spectra, a Thermo Scientific Nicolet iZ10 equipment with a DTGS detector and diamond ATS was used.[39]

Differential scanning calorimetry (DSC) thermograms were obtained using perforated aluminum capsules with a Mettler-Toledo (Barcelona, Spain) DSC 823e equipment. The experiment was conducted within a temperature range of 25°C to 140°C, with a temperature increase of 10°C per minute.[16]

In vitro Drug Release

The in vitro study of RLZ release from pVEC-PEG-PLGA-RLZ NPs was evaluated by direct dialysis while maintaining sink conditions. The molecular weight cutoff (MWCO) of 100 KDa allows RLZ (~234 Da) to diffuse through the membrane, while larger components like the nanoparticles are retained within the cassette. To study the release kinetics of RLZ from the nanoparticles, 200 μL samples were taken from the dialysis medium at different timepoints and replaced with 200 μL of fresh medium, maintaining the concentration gradient and sink conditions to ensure continuous diffusion of RLZ. Each dialysis cassette was maintained at 37°C under magnetic stirring. Finally, each sample was quantified by HPLC and the data obtained were analyzed and fitted to kinetic models using GraphPad Prism version 9.0 software.[16,18,40]

Pharmacokinetic Profile and Biodistribution Assays in vivo

To evaluate the pharmacokinetic profile, an intraperitoneal injection of either free RLZ dissolved after a sonication process at a concentration of 1.5 mg/mL in a 3.5% aqueous solution of Tween 80® or pVEC-RLZ-NP (10 mg RLZ/kg body weight) was administered to 6-month WT C57BL/6 female mice (n = 3 for each condition). Mice were kept under standard conditions and handled in accordance with the guidelines of the European Union Council (Directive 2010/63/EU) and Spanish regulations on the use of laboratory animals. Experimental procedures were approved by the Ethics Committee of the Universitat de Barcelona (CEEA: 355/23).

After being anesthetized with isoflurane, an intracardiac puncture was applied for blood extraction at predetermined timepoints (1, 4, 8, 16, 20, 24 and 48 h), and animals were euthanized. Afterwards, brain, liver, pancreas, lungs and kidneys were removed. All organs were weighed previous to quantify RLZ, using an optimized LC-MS-MS method with the addition of Riluzole ^{13}C ^{15}N as internal standard (IS).[41] In order to process the samples prior to LC-MS-MS, tissues were homogenized with the IS and ethyl acetate to extract RLZ.[42] Samples were centrifuged at 17.000 g for 20 minutes at 4°C. The supernatant was collected, and ethyl acetate was evaporated. Samples were resuspended in methanol : H_2O (80:20) with 0.1% TFA.

For RLZ quantification in plasma, it was previously separated by centrifugation and then RLZ was extracted from 200 μL samples. IS was added following the same procedure. All determinations were performed by triplicate.

In vivo Distribution of Fluorescently Labeled pVEC-PEG-PLGA-RLZ NPs

The brain and spinal cord biodistribution studies were performed after single intraperitoneal administration (10 mg RLZ/kg body weight). Mice were kept under standard conditions and handled in accordance with the guidelines of the European Union Council (Directive 2010/63/EU) and Spanish regulations on the use of laboratory animals. All experimental procedures were approved by the Ethics Committee of the Universitat Autònoma de Barcelona (CEEAH: 9886).

pVEC-PEG-PLGA-RLZ NPs were covalent fluorescently labeled as previously described[43] with Rhodamine 6G or Rhodamine B, for brain and spinal cord studies, respectively, to minimize potential interference with other fluorescent dyes used in the study. NPs targeting to spinal cord were evaluated in SOD1^{G93A} mice (female transgenic mice carrying the G93A human SOD1 mutation B6SJL-Tg [SOD1-G93A]1Gur, aged 6 months) were used as the ALS model, and non-

transgenic WT (female, aged 6 months, n = 3 for each condition). Non-transgenic WT mice were used as negative control after administration of physiological saline (CTL).

After 1 or 24 h post-administration of fluorescent pVEC-PEG-PLGA-RLZ NPs, mice were anesthetized with intraperitoneal injection of pentobarbital (80 mg/kg) and fixed by cardiac perfusion with 4 % paraformaldehyde (PFA) diluted in 0.1 M phosphate buffer. Brain and spinal cord tissues were postfixed for 2 h in 4% PFA solution and then switched to 30 % (w/v) sucrose solution in PBS with 0.01% sodium azide. Transversal spinal cord slices of 20 μm thickness were made on a cryostat. Staining of MNs was carried out by incubating with FluoroNissl Green (1:200, 990210, Invitrogen, California, United States) for 30 minutes at room temperature, and the slides were mounted with Fluoromount G. DAPI was added to label the nuclei. To demonstrate the biodistribution of the fluorescently labeled nanoparticles, images of the spinal cord ventral horn samples were captured at both 20x and 40x under identical sensitivity and exposure time conditions for each marker analyzed.[44] Representative micrographs were obtained using a confocal microscope (LSM 700 Axio Observer, Carl Zeiss), and the conditions were also maintained for subsequent analysis with the ImageJ software.[44]

Statistical Analysis

All data were analyzed using GraphPad Prism 10.0.3 software. Animals were randomized using the randomization calculator provided by GraphPad to ensure equitable allocation and minimize selection bias. Statistical significance was assessed using Student's *t*-test and two-way analysis of variance (ANOVA), both conducted within the GraphPad software, followed by Tukey post-hoc analysis.

Results and Discussion
PLGA Functionalization with PEG and pVEC

PLGA was functionalized prior to NPs production using PEG and pVEC. Firstly, PLGA was attached to PEG. The overall yield of PLGA-PEG synthesis after freeze-drying was over 98% (Figure S1). These results are slightly higher than the yield observed in other studies, ranging from 71.0% to 90.1%.[30,45,46] After ^{1}H-NMR characterization, it can be observed that the polymer obtained presents characteristic peaks of CH_3-PEG-NH_2 at 3.64 ppm, corresponding to the CH_2 protons of the ethylene glycol, as well as peaks of CH_3 and CH group protons of the lactic acid monomer at 1.74 ppm and 5.21 ppm, respectively. The absence of the peak in the region 2.7 corresponding to the N-Hydroxysuccinimide group (NHS), is indicative of the correct pegylation process[47] (Figure S2).

Moreover, pVEC (amino acid sequence: LLIILRRRIRKQAHAHSK**C**) was custom-synthesised by solid-phase peptide synthesis by incorporating a C-terminal cysteine residue that allowed the binding of the peptide to the PLGA maleimide group.[31] Before its covalent linking, pVEC was characterized by electrospray ionization mass spectrometry (ESI-MS) presenting the following m/z ratios corresponding to $[M+5H]^{5+} = 463.46$, $[M+4H]^{4+} = 578.96$, $[M+3H]^{3+} = 771,61$ and $[M+2H]^{2+} = 1156.91$ which are in accordance with the predicted theoretical values, thus confirming the correct synthesis of the peptide (Figure S3). Afterwards, pVEC was covalently attached to PLGA obtaining a conjugation yield around 86%, a high percentage considering the different hydrophilicity-hydrophobicity of these polymers. ^{1}H-NMR analysis of pVEC-PLGA evidenced the binding of the polymer to CPP. As it can be observed in Figure 1A, PLGA-Mal, apart from the characteristic peaks of PLGA, presented a peak at 7.02 corresponding to the maleimide group. In Figure 1B, several peaks in the region between 6.80 and 8.58 ppm corresponding to the protons of the aromatic tryptophan groups of pVEC can be observed.[25,30,48] Finally, in Figure 1C, corresponding to PLGA-pVEC, the characteristic peaks of both PLGA and pVEC are observed (1.48 ppm, 3.51 ppm, 4.73–5.34 ppm, 6.80–8.58 ppm). Moreover, the disappearance of the peak corresponding to the CH of the maleimide group at 7.02 ppm is confirmed, indicating the complete incorporation of the peptide into the polymer.[31] These results are also corroborated by the fact that no traces of pVEC were detected in the supernatant measured by HPLC after centrifugation..
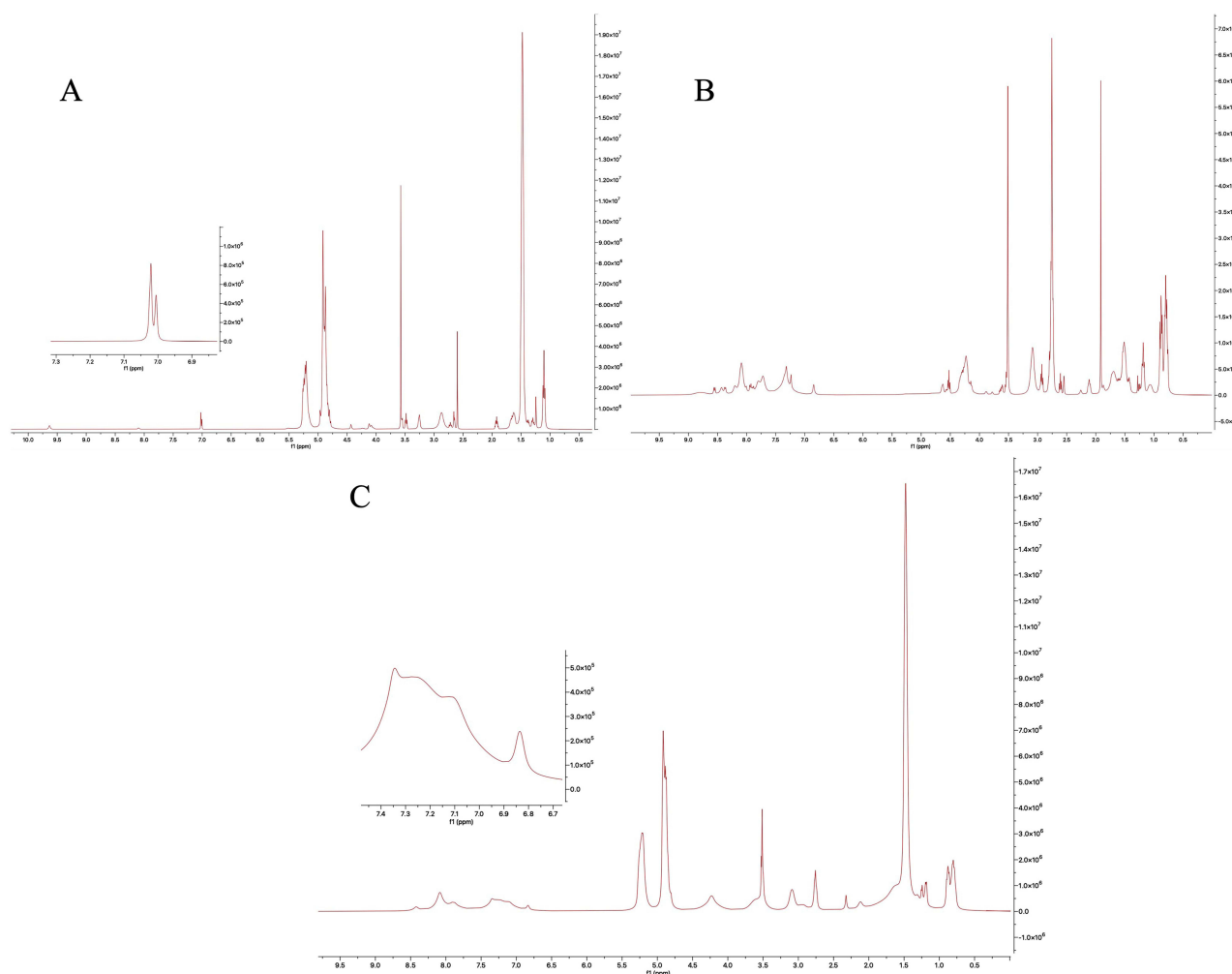
Figure 1 ^{1}H-NMR spectra of: (**A**) PLGA-MAL, (**B**) pVEC, (**C**) PLGA-pVEC.

Physicochemical Characterization of pVEC-PEG-PLGA-RLZ NPs

A nanotechnological platform based on PLGA NPs loading RLZ was optimized in previous studies.[16] From here, two additional targeting strategies have been employed by adding PEG and pVEC to the NPs surface obtaining pVEC-PEG-PLGA-RLZ NPs. These NPs have been characterized in terms of Z_{av}, PI, ZP and EE and compared with the previously developed PLGA-RLZ NPs (Table S1).

pVEC-PEG-PLGA-RLZ NPs showed a Z_{av} of 164.0 ± 1.4 nm, thus demonstrating a statistically significant increase (p < 0.0001) after surface functionalization but still being smaller than 200 nm.[23,49] The PI value was the only parameter that did not show a statistically significant modification after functionalization of the optimized formulation (0.115 ± 0.005) remaining between the range of monomodal systems, thus indicating uniformly functionalized nanoparticles (Figure S4).[50,51] In contrast, zeta potential (ZP) for pVEC-PEG-PLGA-RLZ NPs was +19.2 ± 0.2 mV. This modification of the surface charge is indicative that pVEC has been incorporated on the surface of the NPs, due to the fact that it is an amphipathic-cationic CPP in which more than 40% of the amino acids present a positive charge.[52] This positive charge allows NPs to interact electrostatically with the BBB, specifically with the sialic acid residues of the glycoproteins found in the anionic domains of the luminal surface of the capillaries that form the BBB, favoring adsorption-mediated endocytosis.[22,26,53] In addition, due to NPs physicochemical properties as well as PEG coating, these NPs may have a lower clearance by the reticuloendothelial system.[20] Finally, EE also increases in a significant manner (p < 0.001) up to 95.2 ± 0.4%. This effect may be due to the fact that reversing the charge of the NPs improves interactions with RLZ.

Morphological Characterization

Morphological properties of pVEC-PEG-PLGA-RLZ NPs were also examined by means of transmission electron microscopy (TEM). Moreover, TEM micrograph results (Figure 2) revealed that pVEC-PEG-PLGA-RLZ NPs presented a spherical shape and a size 90.3 ± 10.1 nm, which corroborated the results confirming that average size was below 200 nm.[54]
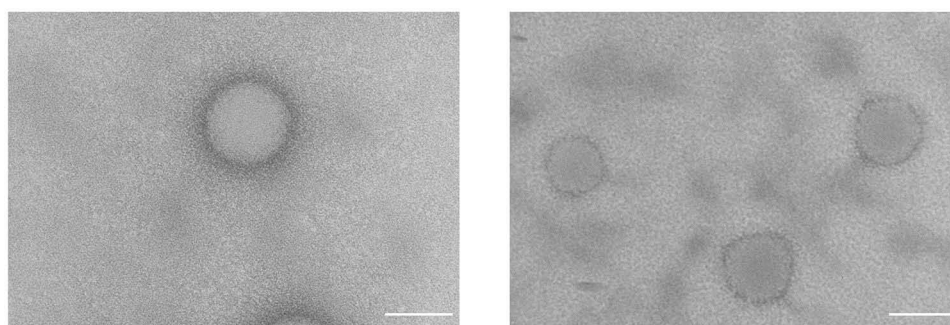
Interaction Studies

In order to observe possible interactions between the components of pVEC-PEG-PLGA-RLZ NPs, several techniques were used.

XRD was used to study the diffraction pattern of pVEC-PEG-PLGA-RLZ NPs. These results are illustrated in Figure 3A, revealing an amorphous pattern characteristic of PLGA[18] whereas RLZ exhibited a crystalline structure, with prominent and pronounced peaks.[34,55] pVEC-PEG-PLGA-RLZ NPs share similarities with the amorphous pattern of polymers such as PLGA, PLGA-PEG or PLGA-Mal, with no discernible peaks corresponding to RLZ, which may indicate that RLZ is molecularly dispersed within the NPs.[56]

Results from FTIR are shown in Figure 3B. Regarding RLZ, the presence of two primary bands can be observed, a broader band located at 3077 cm^{-1} and a narrower one at 3358 cm^{-1}. These may be indicative of the elongation of the primary amine group (N-H).[16] Additionally, a number of peaks aligned with the benzothiazole aromatic ring of RLZ were detectable within the range of 813 to 871 cm^{-1}, thus characteristic of the C-H bending, as well as in the range of 1458 to 1630 cm^{-1}, indicative of C=C and C=N stretching. Furthermore, the presence of the C-F$_3$ group is clear within the absorption peak range from 1230 to 1410 cm^{-1}. Regarding the different polymers PLGA, PLGA-pVEC, PLGA-PEG and PLGA-MAL they presented similar vibrations, with a characteristic peak observed at 1749 cm^{-1}, corresponding to the vibration of the carboxylic group (C=O).[57,58] Additionally, absorptions attributed to the CH$_3$ groups of lactic acid appear at approximately 3016 cm^{-1} and 2926 cm^{-1}, while the absorption related to the CH$_2$ groups of glycolic acid is observed at around 2965 cm^{-1}. Vibrations associated with various C-O, = CO, and C-O-C bonds are also noticeable within the range of 1051–1103 cm^{-1}, along with the 1282–1480 cm^{-1} band which comes from alkene groups. The peak observed at 3090 cm^{-1} corresponds to a characteristic absorption of the hydroxyl group. Furthermore, in the case of PLGA-pVEC, the presence in 1566 cm^{-1} and 1621–1650 cm^{-1} of the characteristic peaks of pVEC due to the bending of the N-H and C-N groups together with those of PLGA are observed, which confirms the correct coupling of the peptide with the polymer. All peaks observed in the spectrum correspond to those described in literature.[59] pVEC-PEG-PLGA-RLZ NPs spectrum showed almost the same pattern as polymers indicating that there were no covalent bond between polymeric matrix and RLZ, due to the fact that they may interact through weak forces such as hydrogen bonds or Van der Waals.[29,35]

Thermal profile was assessed by DSC, and the thermograms obtained are shown in Figure 3C. RLZ thermogram revealed a distinct peak corresponding to the melting temperature (T$_m$) at 118.54°C with an associated enthalpy of 79.93 J/g. Moreover, PLGA exhibited its glass transition temperature (T$_g$) at 54.12°C and an associated enthalpy of 5.83. It should be noted that due to the addition of PEG to PLGA, the intensity of the peak was diminished.[60] Furthermore, the other components did not

Figure 2 Transmission electron microscopy images of pVEC-PEG-PLGA-RLZ NPs (scale bar 100 nm).
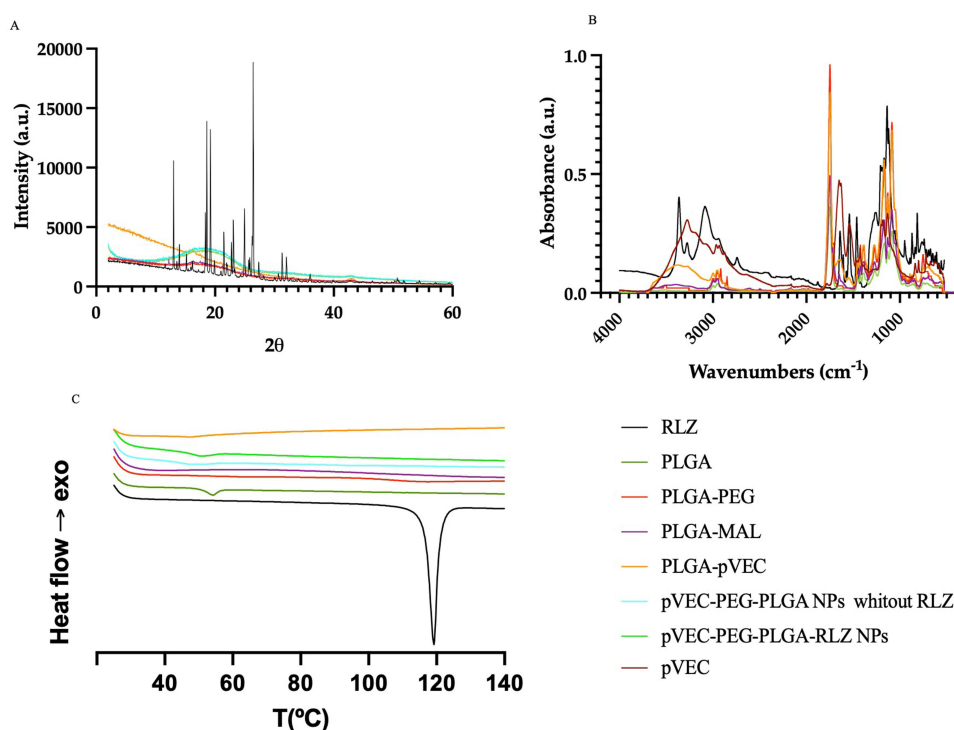
Figure 3 Interaction studies for pVEC-PEG-PLGA-RLZ NPs optimized formulation and their components (**A**); XRD diffraction patterns. (**B**) FTIR profile. (**C**) DSC thermal profile.

present a phase change and for this reason they do not present a remarkable enthalpic change. Furthermore, RLZ melting peak is not observed in pVEC-PEG-PLGA-RLZ NPs that corroborates its encapsulation in the polymeric matrix.[16,61,62]

In vitro Drug Release

One of the aims for the development of pVEC-PEG-PLGA-RLZ NPs was to obtain a prolonged RLZ release over time. The in vitro RLZ release kinetic profile of pVEC-PEG-PLGA-RLZ NPs (Figure 4) demonstrates that they allow a sustained release. Moreover, data were adjusted to the most common kinetic models obtaining the best fit with the Korsmeyer-Peppas kinetic model ($r^2 = 0.9911$), with a release constant rate (K) of 0.4591. This model is usually used to describe the drug release behavior of polymeric nanoparticles.[55,63] At 24 h, the nanoparticles released 55% of the encapsulated drug, which is 35% less compared to the free drug.
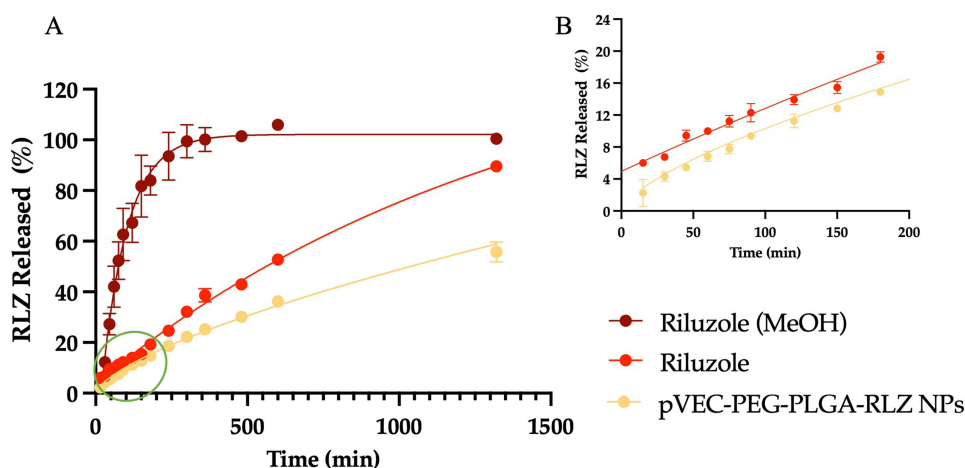

Figure 4 (**A**): In vitro drug release profile of the free Riluzole and pVEC-PEG-PLGA-RLZ NPs, (**B**) Zoom of the corresponding section 0 to 200 min.

Moreover, free RLZ was not completely released after 24 h, according to methodology used, due to the presence of Tween 80® in the dialysis medium. This has been reported in previous work,[16] since this surfactant contains hydrophobic regions that can delay release. The kinetic model that best adjusted to free RLZ pattern was the one phase decay model (r^2 = 0.9944). pVEC-PEG-PLGA-RLZ NPs, compared with the free RLZ, were capable of delaying RLZ release (Figure 4). In order to confirm Tween 80® effect, an additional release of free RLZ in methanol was also performed. In the initial timepoints, there was a greater difference between free RLZ in Tween 80® and in methanol thus confirming the capacity of this surfactant to delay the release.[16,64]

Pharmacokinetics and Biodistribution Studies

In order to elucidate the pharmacokinetics of pVEC-PEG-PLGA-RLZ NPs, a single dose of RLZ or pVEC-PEG-PLGA-RLZ NPs (10 mg/kg) was administered to wild type C57BL/6 (WT) mice and RLZ was quantified in several organs at predetermined timepoints. Results showed that, after 1 h, the concentration of RLZ in brain derived from pVEC-PEG-PLGA-RLZ NPs was significantly higher than that of free RLZ ($p < 0.01$) (Figure 5A). Interestingly, contrasting trends were observed in the other examined tissues, with statistically significant differences in RLZ concentration noted after 1 h of administration in nearly all organs. Notably, the central nervous system (CNS) exhibited a higher concentration of RLZ resulting from the developed NPs formulation compared to the free drug, distinguishing it as the sole organ to display this characteristic. Due to the functionalization of pVEC-PEG-PLGA-RLZ NPs, a favorable cumulative drug concentration ratio was achieved in the brain with respect to other organs, such as the liver. In this case, RLZ ratio for pVEC-PEG-PLGA-RLZ NPs ([RLZ liver]/[RLZ brain]) was 2.04, in contrast, for free RLZ, this ratio was 3.81. After 24 h, this trend was maintained with a ratio of 15.91 for pVEC-PEG-PLGA-RLZ NPs and 34.52 for the free RLZ (Figure 5B). In other experimental studies, it is described how controlled release systems of similar drugs with a size above 150 nm are recognized by the reticuloendothelial system and accumulate in the liver to be eliminated.[65–67] Regarding pVEC-PEG-PLGA-RLZ NPs, due to their multifunctionalization (PEG reduces recognition by the
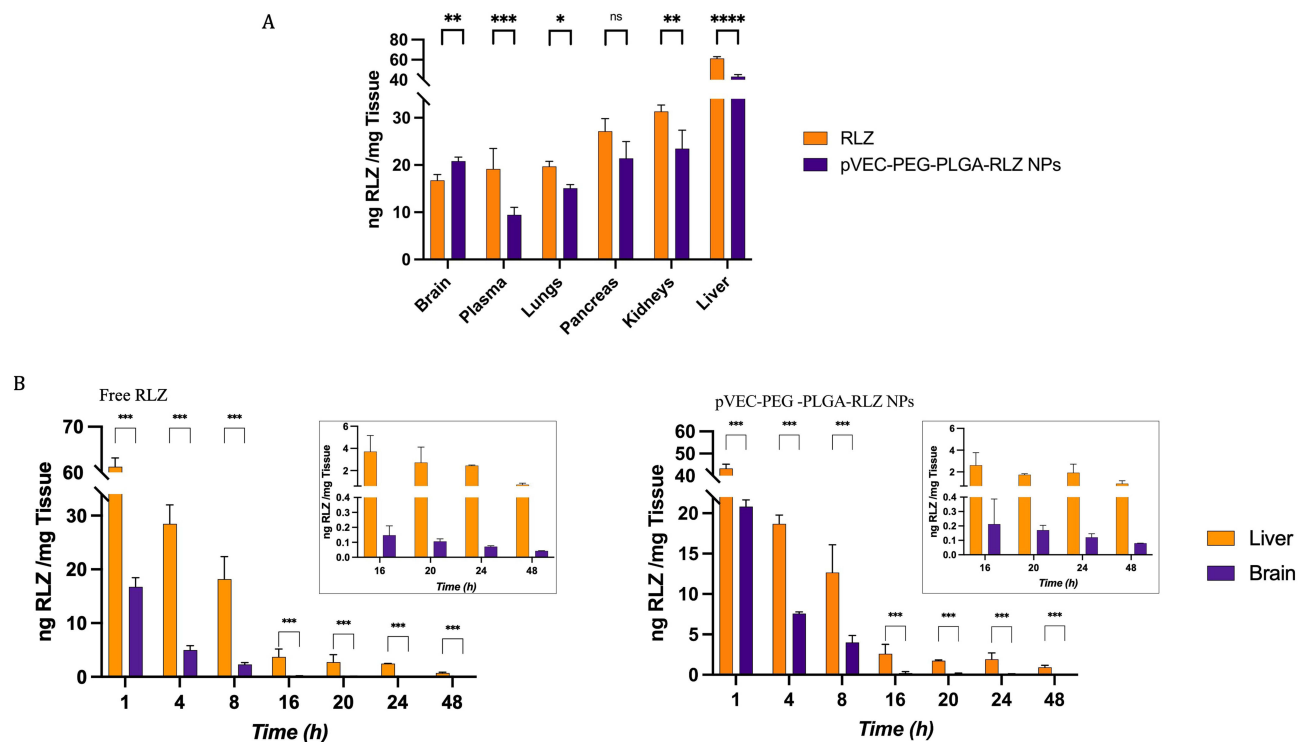

Figure 5 Pharmacokinetics and biodistribution studies (**A**) Concentration of RLZ after 1 h of the administration of the optimized formulations under study (**B**) Comparative diagrams of RLZ brain and liver concentration of free RLZ and pVEC-PEG-PLGA-RLZ NPs. * p- <0.05, ** p <0.01, *** p <0.001,**** p <0.0001.

reticuloendothelial system and pVEC allows penetration into the CNS reducing liver accumulation) this may translate into a potential reduction of the intrinsic hepatotoxicity of RLZ, while increasing the concentration in the CNS.

Regarding the pharmacokinetic profile in plasma, the maximum concentration occurred after 1 h for both free RLZ and pVEC-PEG-PLGA-RLZ NPs. From 8 h onwards, RLZ concentration of pVEC-PEG-PLGA-RLZ NPs in plasma was higher than that of the free RLZ, and from 16 h onwards significant differences were obtained ($p < 0.001$). These results are probably due to the sustained release of RLZ from pVEC-PEG-PLGA-RLZ NPs and their PEG functionalization avoiding fast clearance. It is relevant to highlight that after 48 h, free RLZ was not detected (<0.01 ng/mg), while pVEC-PEG-PLGA-RLZ NPs treated mice showed plasma levels around 0.0135 ng/mL (Figure 6A).

The pharmacokinetic profile of the free drug and pVEC-PEG-PLGA-RLZ NPs in the brain exhibited similarities, with both reaching maximum drug concentration 1 h after administration (Figure 6B). However, pVEC-PEG-PLGA-RLZ NPs showed higher and more stable RLZ concentrations. After 24 h, the concentration of free RLZ was 0.0428 ± 0.0016 ng/mg while for pVEC-PEG-PLGA-RLZ NPs it was 0.0798 ± 0.0013 ng/mg. Furthermore, the area under curve (AUC) corroborates these significant differences with a value of 59.16 ± 3.687 h·ng/mg for the free drug and 86.43 ± 4.196 h·ng/mg for the pVEC-PEG-PLGA-RLZ NPs.

Pharmacokinetic profiles of other organs evaluated, such as lung, kidney, pancreas or liver show AUC values of free RLZ higher than pVEC-PEG-PLGA-RLZ NPs (Figure 7). For instance, on the liver, free RLZ AUC was 376.82 ± 30.34 h·ng/mg, while for pVEC-PEG-PLGA-RLZ NPs it was 266.91 ± 22.75 h·ng/mg. It can be observed that in all the organs evaluated except the brain, the concentration of RLZ of the animals treated with free RLZ was greater compared to the animals treated with drug loaded NPs. As plasma levels indicate, at further timepoints, free RLZ is eliminated but with pVEC-PEG-PLGA-RLZ NPs either equal or slightly higher concentrations are achieved. However, these differences in latter timepoints were not significant. This is attributed to the fact that RLZ, being protected within the polymeric
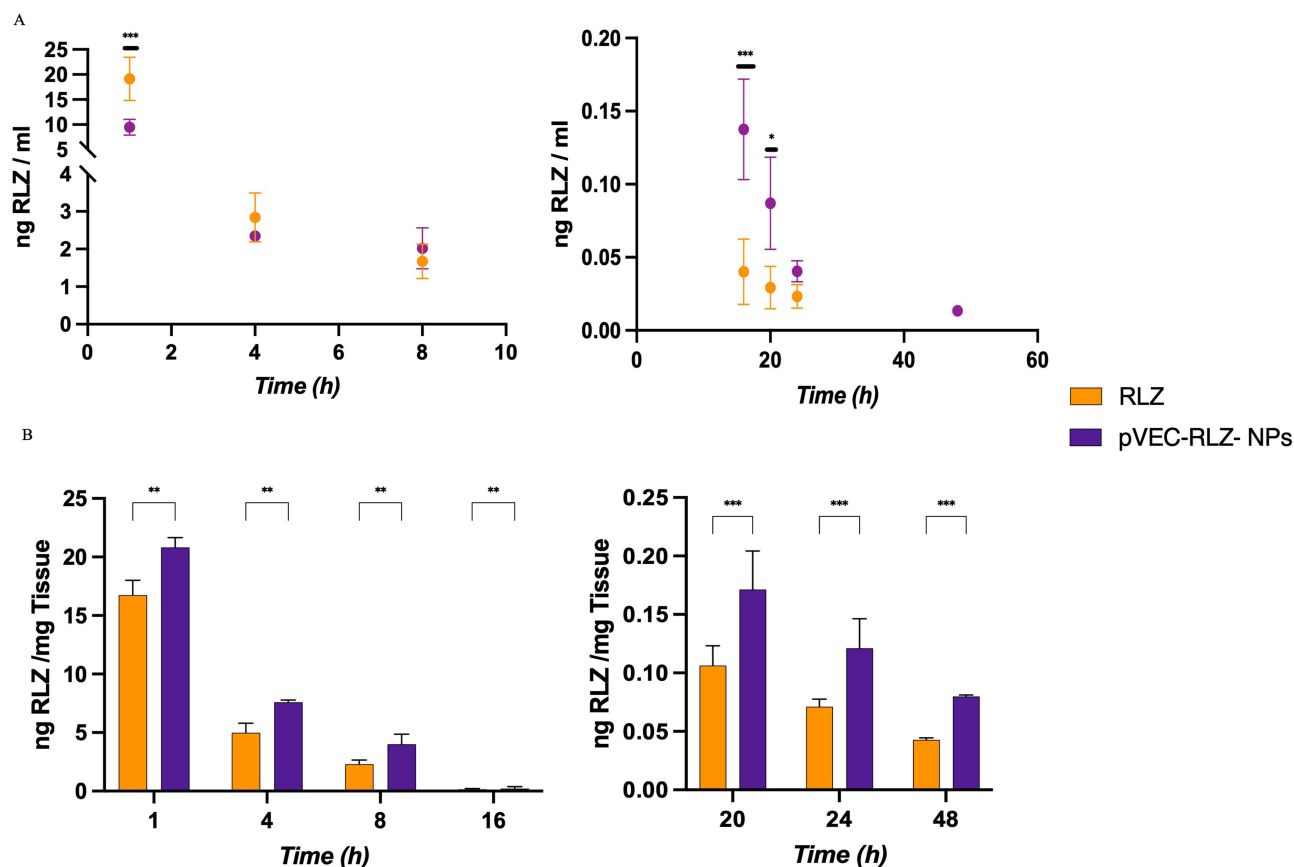
Figure 6 Pharmacokinetic profile of RLZ obtained after intraperitoneal injection of free RLZ and pVEC-PEG-PLGA-RLZ NPs in (**A**): Plasma, (**B**): Brain. * p value <0.05, ** p value <0.01, *** p value <0.001.
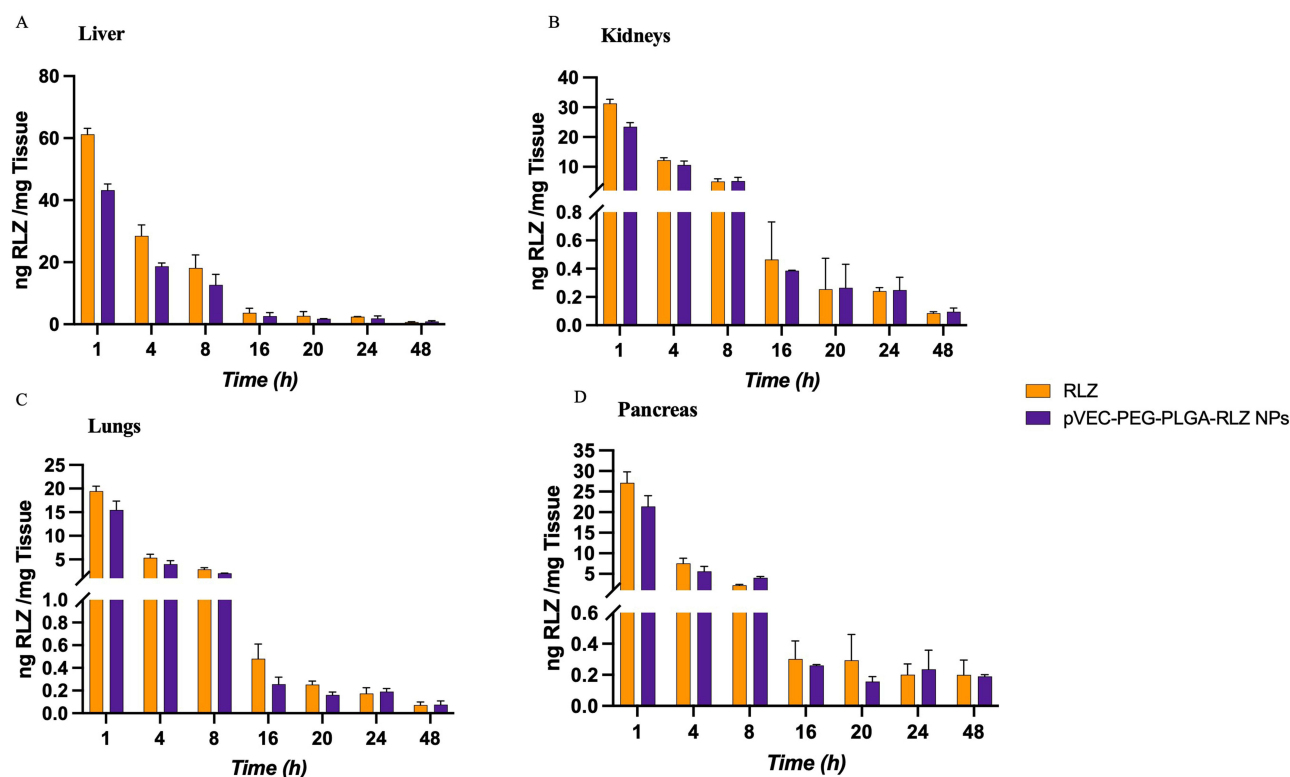
Figure 7 Pharmacokinetics of RLZ in several organs after intraperitoneal injection. (**A**) Liver, (**B**) Kidneys, (**C**) Lungs and (**D**) Pancreas.

matrix and released in a sustained manner, may allow for the maintenance of a higher concentration of the drug in the organism over time and finally its elimination.

Spinal Cord and Brain Localization of Labeled Nanoparticles

pVEC-PEG-PLGA-RLZ NPs were fluorescently labeled with Rhodamine B or Rhodamine 6G and administered intraperitoneally (10 mg/Kg) to both WT and SOD1^G93A mice at the symptomatic stage of ALS disease, 16 weeks of age. Results showed that Rho-pVEC-PEG-PLGA-RLZ NPs were able to cross the BBB in WT mice being present in the hippocampus, specifically in the dentate gyrus, as well as in both the primary and secondary somatomotor cortex only 1 h after administration (Figure 8A). This fact is of special importance because it indicates that pVEC-PEG-PLGA-RLZ NPs can penetrate into the CNS.

Furthermore, after intraperitoneal single administration of Rho-pVEC-PEG-PLGA-RLZ NPs in WT and SOD1^G93A mice, fluorescence was observed both after 1 h and 24 h post-administration (Figure 8B). Rho-pVEC-PEG-PLGA-RLZ NPs were detected mainly into the MNs of the spinal cord lumbar sections, demonstrating that Rho-pVEC-PEG-PLGA-RLZ NPs in a short period of time can reach the target of the MNDs in WT and in ALS mice.

Moreover, these results also highlight that pVEC-PEG-PLGA-RLZ NPs after 24 h are still present at the level of the spinal cord, presenting greater fluorescence than after 1 h. Furthermore, internalized Rho-pVEC-PEG-PLGA-RLZ NPs can be observed both at perinuclear and at the cytoplasmic level, which is of special interest for drugs such as RLZ due to its mechanisms of action (Figure 8).[8–11]

These results demonstrate that Rho-pVEC-PEG-PLGA-RLZ NPs were able to cross the BBB and reach therapeutic concentrations in the brain while reducing drug exposure and accumulation in other organs such as the liver. In addition, their controlled release allows them to maintain prolonged plasma levels and improve drug efficacy. These findings support the potential of pVEC-PEG-PLGA-RLZ NPs as an effective and selective drug delivery system for the treatment of MNDs.
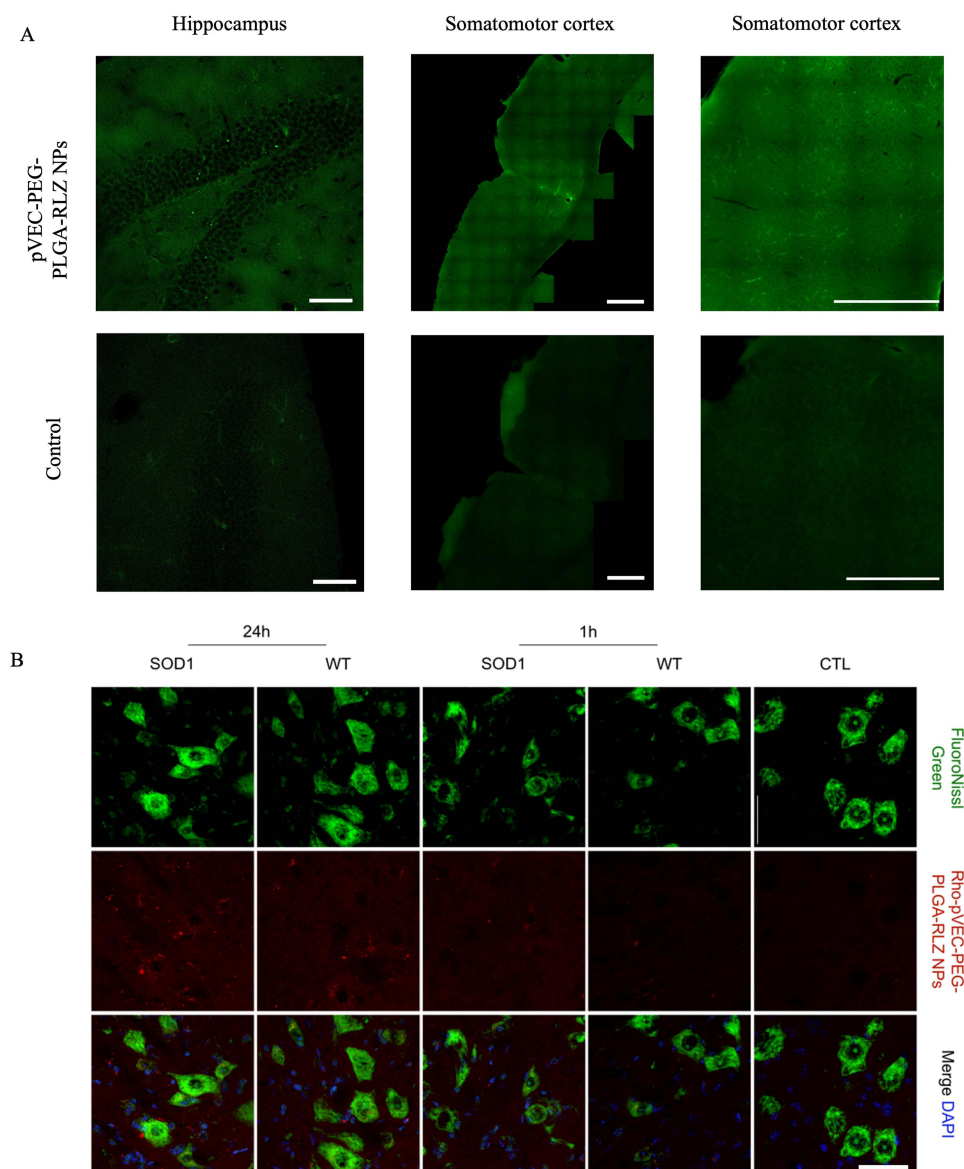
Figure 8 Biodistribution of fluorescently labeled pVEC-PEG-PLGA-RLZ NPs, (**A**) Dentate gyrus of the hippocampus (Scale bar 50 μm) and Somatomotor Cortex (Scale bar 500 μm), (**B**) Representative images of spinal cord lumbar sections stained with Fluoro Nissl Green (Scale bar 50 μm).

Conclusion

In this study, we developed and characterized a novel tissue-specific multifunctionalized polymeric nanoparticles encapsulating RLZ. This formulation utilizes both Tween 80® and PEG for passive targeting and pVEC, a CPP, to enhance transport and reach targets related to MND, thereby providing active targeting. pVEC-PEG-PLGA-RLZ NPs were developed and physicochemically characterized, achieving suitable surface functionalization, high RLZ yield, and excellent physicochemical properties. Moreover, the NPs were able to release RLZ in a prolonged manner. Our results indicate that these novel formulation significantly improved the pharmacokinetic profile and biodistribution of RLZ. We observed that 1 h after intraperitoneal administration in rodents, nanoparticles were present in motor neurons, facilitating sustained release of RLZ in the therapeutic target cells while reducing its concentration in organs associated with adverse effects. In summary, our findings suggest that the biodegradable and biocompatible multifunctionalized RLZ nanoparticles developed in this study may serve as a promising system for delivering this drug to the central nervous system

(CNS) and specifically targeting motor neurons. This enhanced selectivity may offer important implications for the future treatment of motor neuron diseases.

Ethics Statement

Acknowledgments

Author Contributions

All authors made a significant contribution to the work reported, whether that is in the conception, study design, execution, acquisition of data, analysis and interpretation, or in all these areas; took part in drafting, revising or critically reviewing the article; gave final approval of the version to be published; have agreed on the journal to which the article has been submitted; and agree to be accountable for all aspects of the work.

Funding

Disclosure

The authors declare no competing interests.

References

1. Gagliardi D, Pagliari E, Meneri M, et al. Stathmins and motor neuron diseases: pathophysiology and therapeutic targets. *Biomedicines*. 2022;10 (3):1–10. doi:10.3390/biomedicines10030711
2. Ricci G, Torri F, Bianchi F, et al. Frailties and critical issues in neuromuscular diseases highlighted by SARS-CoV-2 pandemic: how many patients are still "invisible"? *Acta Myol*. 2022;41(1):24–29. doi:10.36185/2532-1900-065
3. Park J, Kim JE, Song TJ. The global burden of motor neuron disease: an analysis of the 2019 global burden of disease study. *Front Neurol*. 2022;13:1–15. doi:10.3389/fneur.2022.864339
4. Garg N, Park SB, Vucic S, et al. Differentiating lower motor neuron syndromes. *J Neurol Neurosurg Psychiatry*. 2017;88(6):474–483. doi:10.1136/jnnp-2016-313526
5. Breza M, Koutsis G. Kennedy's disease (spinal and bulbar muscular atrophy): a clinically oriented review of a rare disease. *J Neurol*. 2019;266 (3):565–573. doi:10.1007/s00415-018-8968-7
6. Zhang X, Yang K, Le W. Autophagy and motor neuron diseases. In: Le W, editor. *Autophagy Biol Dis Clin Sci*. Springer; 2020:53–75.
7. Masrori P, Van Damme P. Amyotrophic lateral sclerosis: a clinical review. *Eur J Neurol*. 2020;27(10):1918–1929. doi:10.1111/ene.14393
8. Fumagalli E, Funicello M, Rauen T, Gobbi M, Mennini T. Riluzole enhances the activity of glutamate transporters GLAST, GLT1 and EAAC1. *Eur J Pharmacol*. 2008;578(2–3):171–176. doi:10.1016/j.ejphar.2007.10.023
9. Pirhan D, Yüksel N, Emre E, Cengiz A, Kürşat Yildiz D. Riluzole- and resveratrol-induced delay of retinal ganglion cell death in an experimental model of glaucoma. *Curr Eye Res*. 2016;41(1):59–69. doi:10.3109/02713683.2015.1004719
10. Povedano-Panades M, Couratier P, Sidle K, Sorarù G, Tsivgoulis G, Ludolph AC. Administration of Riluzole oral suspension during the different stages of amyotrophic lateral sclerosis. *Front Neurol*. 2021;12:10–13. doi:10.3389/fneur.2021.633854
11. Andrews JA, Jackson CE, Heiman-Patterson TD, Bettica P, Brooks BR, Pioro EP. Real-world evidence of riluzole effectiveness in treating amyotrophic lateral sclerosis. *Amyotroph Lateral Scler Front Degener*. 2020;21(7–8):509–518. doi:10.1080/21678421.2020.1771734
12. Miller RG, Mitchell JD, Lyon M, Moore DH. Riluzole for amyotrophic lateral sclerosis (ALS)/motor neuron disease (MND). *Cochrane Database Syst Rev*. 2012;3 doi:10.1002/14651858.CD001447.pub3.
13. Zarate C. Riluzole in Psychiatry. *Occup Env Med*. 2008;23:1–7.

14. Inoue-Shibui A, Kato M, Suzuki N, et al. Interstitial pneumonia and other adverse events in riluzole-administered amyotrophic lateral sclerosis patients: a retrospective observational study. *BMC Neurol*. 2019;19(1):3–9. doi:10.1186/s12883-019-1299-1

15. Saitoh Y, Aoshima Y, Mukai T, et al. Riluzole-induced interstitial lung disease is a rare and potentially life-threatening adverse event successfully treated with high-dose steroid therapy: case reports and review of the literature. *J Neurol Sci*. 2020;410:116650. doi:10.1016/j.jns.2019.116650

16. Esteruelas G, Halbaut L, García-Torra V, et al. Development and optimization of Riluzole-loaded biodegradable nanoparticles incorporated in a mucoadhesive in situ gel for the posterior eye segment. *Int J Pharm*. 2022;612 doi:10.1016/j.ijpharm.2021.121379.

17. Xu R, Wang J, Xu J, et al. Rhynchophylline loaded-mPEG-PLGA nanoparticles coated with tween-80 for preliminary study in Alzheimer's disease. *Int J Nanomed*. 2020;15:1149–1160. doi:10.2147/IJN.S236922

18. Sánchez-López E, Ettcheto M, Egea MA, et al. New potential strategies for Alzheimer's disease prevention: pegylated biodegradable dexibuprofen nanospheres administration to APPswe/PS1dE9. *Nanomedi Nanotechnol, Biol Med*. 2017;13(3):1171–1182. doi:10.1016/j.nano.2016.12.003

19. Sánchez-López E, Esteruelas G, Ortiz A, et al. Article dexibuprofen biodegradable nanoparticles: one step closer towards a better ocular interaction study. *Nanomaterials*. 2020;10(4):1–24. doi:10.3390/nano10040720

20. Gao H, Liu J, Yang C, et al. The impact of PEGylation patterns on the in vivo biodistribution of mixed shell micelles. *Int J Nanomed*. 2013;8:4229–4246. doi:10.2147/IJN.S51566

21. Li Z, Zhu Y, Zeng H, et al. Mechano-boosting nanomedicine antitumour efficacy by blocking the reticuloendothelial system with stiff nanogels. *Nat Commun*. 2023;14(1):1–18. doi:10.1038/s41467-022-34464-6

22. Esteruelas G, Souto EB, Cano A, et al. Chapter 5 - Polymeric nanoparticles as drug delivery systems for dementia. In: Gupta U, Kesharwani P, editors. *Nanomedicine-Based Approaches Treat Dement*. Academic Press; 2023: doi:10.1016/B978-0-12-824331-2.00006-6 89–114.

23. Silva S, Almeida AJ, Vale N. Combination of cell-penetrating peptides with nanoparticles for therapeutic application: a review. *Biomolecules*. 2019;9(1):22. doi:10.3390/biom9010022

24. Tabujew I, Lelle M, Peneva K. Cell-penetrating peptides for nanomedicine-how to choose the right peptide. *BioNanoMaterials*. 2015;16(1):59–72. doi:10.1515/bnm-2015-0001

25. Falanga A, Lombardi L, Galdiero E, Genio VD, Galdiero S. The world of cell penetrating: the future of medical applications. *Future Med Chem*. 2020;12(15):1431–1446. doi:10.4155/fmc-2020-0140

26. Stalmans S, Bracke N, Wynendaele E, et al. Cell-penetrating peptides selectively cross the blood-brain barrier in vivo. *PLoS One*. 2015;10 (10):1–22. doi:10.1371/journal.pone.0139652

27. Santos Rodrigues Dos B, Lakkadwala S, Kanekiyo T, Singh J. Development and screening of brain-targeted lipid-based nanoparticles with enhanced cell penetration and gene delivery properties. *Int J Nanomed*. 2019;14:6497–6517. doi:10.2147/IJN.S215941

28. Locatelli E, Franchini MC. Biodegradable PLGA-b-PEG polymeric nanoparticles: synthesis, properties, and nanomedical applications as drug delivery system. *J Nanopart Res*. 2012;14(12):1–17. doi:10.1007/s11051-012-1316-4

29. Elsewedy HS, Dhubiab BEA, Mahdy MA, Elnahas HM. Development, optimization, and evaluation of PEGylated brucine-loaded PLGA nanoparticles. *Drug Deliv*. 2020;27(1):1134–1146. doi:10.1080/10717544.2020.1797237

30. Gonzalez-Pizarro R, Parrotta G, Vera R, et al. Ocular penetration of fluorometholone-loaded PEG-PLGA nanoparticles functionalized with cell-penetrating peptides. *Nanomedicine*. 2019;14(23):3089–3104. doi:10.2217/nnm-2019-0201

31. Vasconcelos A, Vega E, Pérez Y, Gómara MJ, García ML, Haro I. Conjugation of cell-penetrating peptides with poly (Lactic-co-glycolic acid)-polyethylene glycol nanoparticles improves ocular drug delivery. *Int J Nanomed*. 2015;10:609–631. doi:10.2147/IJN.S71198

32. Hansen PR, Oddo A. Fmoc solid-phase peptide synthesis. In: Houen G, editor. *Pept Antibodies Methods Protoc*. New York: Humana Press; 2015: 83–102. http://www.springer.com/gb/book/9781493929986.

33. García-Moreno C, Gómara MJ, Castellanos-Moreira R, Sanmartí R, Haro I. Peptides bearing multiple post-translational modifications as antigenic targets for severe rheumatoid arthritis patients. *Int J mol Sci*. 2021;23(1):22. doi:10.3390/ijms23010022

34. Sánchez López E, Esteruelas G, Ortiz A, et al. Dexibuprofen biodegradable nanoparticles: one step closer towards a better ocular interaction study. *Nanomaterials*. 2020;10(4):1–10 doi:10.3390/nano10040720.

35. Esteruelas G, Souto EB, Espina M, et al. Diclofenac loaded biodegradable nanoparticles as antitumoral and antiangiogenic therapy. *Pharmaceutics*. 2023;16:15. doi:10.3390/pharmaceutics16010015

36. Carvajal-Vidal P, Fábrega MJ, Espina M, Calpena AC, García ML. Development of Halobetasol-loaded nanostructured lipid carrier for dermal administration: optimization, physicochemical and biopharmaceutical behavior, and therapeutic efficacy. *Nanomedi Nanotechnol, Biol Med*. 2019;20:102026. doi:10.1016/j.nano.2019.102026

37. Gonzalez-Pizarro R, Carvajal-Vidal P, Halbault Bellowa L, Calpena AC, Espina M, García ML. In-situ forming gels containing fluorometholone-loaded polymeric nanoparticles for ocular inflammatory conditions. *Colloids Surf B Biointerfaces*. 2019;175:365–374. doi:10.1016/j.colsurfb.2018.11.065

38. López-Machado A, Díaz N, Cano A, et al. Development of topical eye-drops of lactoferrin-loaded biodegradable nanoparticles for the treatment of anterior segment inflammatory processes. *Int J Pharm*. 2021;609:121188. doi:10.1016/j.ijpharm.2021.121188

39. Cano A, Ettcheto M, Espina M, et al. Epigallocatechin-3-gallate loaded PEGylated-PLGA nanoparticles: a new anti-seizure strategy for temporal lobe epilepsy. *Nanomedi Nanotechnol, Biol Med*. 2018;14(4):1073–1085. doi:10.1016/j.nano.2018.01.019

40. Zielinska A, Carreiró F, Oliveira AM, et al. Polymeric nanoparticles: production, characterization, toxicology and ecotoxicology Aleksandra. *Princ Nanomedicine*. 2019;195–240.

41. Eure WD, Grossman RG, Horner PJ, Chow DS-L. LC-MS/MS assay of riluzole and etoricoxib in rat plasma and brain tissue with applications for sampling and evaluation in pre-clinical rat model of traumatic brain injury. *Talanta Open*. 2021;4:100052. doi:10.1016/j.talo.2021.100052

42. Bondì ML, Craparo EF, Giammona G, Drago F. Brain-targeted solid lipid nanoparticles containing riluzole: preparation, characterization and biodistribution. *Nanomedicine*. 2010;5(1):25–32. doi:10.2217/nnm.09.67

43. Elmsmari F, González Sánchez JA, Duran-Sindreu F, et al. Calcium hydroxide-loaded PLGA biodegradable nanoparticles as an intracanal medicament. *Int Endod J*. 2021;54(11):2086–2098. doi:10.1111/iej.13603

44. Gaja-Capdevila N, Hernández N, Navarro X, Herrando-Grabulosa M. Sigma-1 receptor is a pharmacological target to promote neuroprotection in the SOD1G93A ALS mice. *Front Pharmacol*. 2021;12:1–13. doi:10.3389/fphar.2021.780588

45. Zambito G, Deng S, Haeck J, et al. Fluorinated PLGA-PEG-mannose nanoparticles for tumor-associated macrophage detection by optical imaging and MRI. *Front Med*. 2021;8:1–12. doi:10.3389/fmed.2021.712367

46. Gholizadeh S, Kamps JAAM, Hennink WE, Kok RJ. PLGA-PEG nanoparticles for targeted delivery of the mTOR/PI3kinase inhibitor dactolisib to inflamed endothelium. *Int J Pharm*. 2018;548(2):747–758. doi:10.1016/j.ijpharm.2017.10.032

47. Liu CW, Lin WJ. Polymeric nanoparticles conjugate a novel heptapeptide as an epidermal growth factor receptor-active targeting ligand for doxorubicin. *Int J Nanomed*. 2012;7:4749–4767. doi:10.2147/IJN.S32830

48. Madani F, Lindberg S, Langel Ü, Futaki S, Gräslund A. Mechanisms of cellular uptake of cell-penetrating peptides. *J Biophys*. 2011;2011:1–10. doi:10.1155/2011/414729

49. Xie J, Bi Y, Zhang H, et al. Cell-penetrating peptides in diagnosis and treatment of human diseases: from preclinical research to clinical application. *Front Pharmacol*. 2020;11:1–23. doi:10.3389/fphar.2020.00697

50. Song X, Zhao Y, Hou S, et al. Dual agents loaded PLGA nanoparticles: systematic study of particle size and drug entrapment efficiency. *Eur J Pharm Biopharm*. 2008;69(2):445–453. doi:10.1016/j.ejpb.2008.01.013

51. Pinheiro RGR, Granja A, Loureiro JA, et al. RVG29-functionalized lipid nanoparticles for Quercetin brain delivery and Alzheimer's disease. *Pharm Res*. 2020;37(7):139. doi:10.1007/s11095-020-02865-1

52. Akdag IO, Ozkirimli E. The uptake mechanism of the cell-penetrating pVEC peptide. *J Chem*. 2013;2013(1):9. doi:10.1155/2013/851915

53. Frøslev P, Franzyk H, Ozgür B, Brodin B, Kristensen M. Highly cationic cell-penetrating peptides affect the barrier integrity and facilitates mannitol permeation in a human stem cell-based blood-brain barrier model. *Eur J Pharm Sci*. 2022;168.

54. Sánchez-López E, Egea MA, Cano A, et al. PEGylated PLGA nanospheres optimized by design of experiments for ocular administration of dexibuprofen-in vitro, ex vivo and in vivo characterization. *Colloids Surf B Biointerfaces*. 2016;145:241–250. doi:10.1016/j.colsurfb.2016.04.054

55. Pal A, Bajpai J, Bajpai AK. Poly (acrylic acid) grafted gelatin nanocarriers as swelling controlled drug delivery system for optimized release of paclitaxel from modified gelatin. *J Drug Deliv Sci Technol*. 2018;45:323–333. doi:10.1016/j.jddst.2018.03.025

56. Llorente X, Esteruelas G, Bonilla L, et al. Riluzole-loaded nanostructured lipid carriers for hyperproliferative skin diseases. *Int J mol Sci*. 2023;24 (9):8053. doi:10.3390/ijms24098053

57. Forna N, Damir D, Duceac LD, et al. Nano-architectonics of antibiotic-loaded polymer particles as vehicles for active molecules. *Appl Sci*. 2022;12.

58. Zhu D, Zhang WG, Nie XD, Ding SW, Zhang DT, Yang L. Rational design of ultra-small photoluminescent copper nano-dots loaded PLGA micro-vessels for targeted co-delivery of natural piperine molecules for the treatment for epilepsy. *J Photochem Photobiol B: Biol*. 2020;205:1–8. doi:10.1016/j.jphotobiol.2020.111805

59. Gonzalez-Pizarro R, Silva-Abreu M, Calpena AC, Egea MA, Espina M, García ML. Development of fluorometholone-loaded PLGA nanoparticles for treatment of inflammatory disorders of anterior and posterior segments of the eye. *Int J Pharm*. 2018;547(1–2):338–346. doi:10.1016/j.ijpharm.2018.05.050

60. Vega E, Antònia Egea M, Calpena AC, Espina M, Luisa García M. Role of hydroxypropyl-β-cyclodextrin on freeze-dried and gamma-irradiated PLGA and PLGA-PEG diblock copolymer nanospheres for ophthalmic flurbiprofen delivery. *Int J Nanomed*. 2012;7:1357–1371. doi:10.2147/IJN.S28481

61. Nair R, Kumar AC, Priya VK, Yadav CM, Raju PY. Formulation and evaluation of chitosan solid lipid nanoparticles of carbamazepine. *Lipids Health Dis*. 2012;11:11. doi:10.1186/1476-511X-11-11

62. Öztürk AA, Namlı İ, Güleç K, Kıyan HT. Diclofenac sodium loaded PLGA nanoparticles for inflammatory diseases with high anti-inflammatory properties at low dose: formulation, characterization and in vivo HET-CAM analysis. *Microvasc Res*. 2020;130.

63. Scioli Montoto S, Muraca G, Di Ianni M, et al. Preparation, physicochemical and biopharmaceutical characterization of oxcarbazepine-loaded nanostructured lipid carriers as potential antiepileptic devices. *J Drug Deliv Sci Technol*. 2021;63:102470. doi:10.1016/j.jddst.2021.102470

64. Tao X, Li Y, Hu Q, et al. Preparation and drug release study of novel nanopharmaceuticals with polysorbate 80 surface adsorption. *J Nanomater*. 2018;2018:1–11. doi:10.1155/2018/4718045

65. Cano A, Ettcheto M, Chang JH, et al. Dual-drug loaded nanoparticles of Epigallocatechin-3-gallate (EGCG)/Ascorbic acid enhance therapeutic efficacy of EGCG in a APPswe/PS1dE9 Alzheimer's disease mice model. *J Control Release*. 2019;301:62–75. doi:10.1016/j.jconrel.2019.03.010

66. Hoshyar N, Gray S, Han H, Bao G. The effect of nanoparticle size on in vivo pharmacokinetics and cellular interaction. *Nanomedicine*. 2016;11 (6):673–692. doi:10.2217/nnm.16.5

67. Park JK, Utsumi T, Seo YE, et al. Cellular distribution of injected PLGA-nanoparticles in the liver. *Nanomedicine*. 2016;12(5):1365–1374. doi:10.1016/j.nano.2016.01.013